

Supplementary Information

Title Inertial Microfluidics in Non-rectangular Cross-section Microchannels and Manipulation of Accessible Focusing Position

J. Kim, J. Lee, C. Wu, S. Nam, D. Di Carlo and W. Lee*

Fabrication of the side-view channels

We fabricated the separate devices to observe the motion of particles from the top and the side of channels. The top view channels were built by conventional PDMS microchannel fabrication method, i.e., bonding the molded PDMS channel to a slide glass using plasma. The side view channels were built using the top view channels by cutting the channel and lay on the side (Fig. S1). To build the side-view channel, a flat PDMS substrate was prepared (~3-5 mm thick). The PDMS channel was plasma-bonded on the PDMS substrate instead of glass substrate (Fig. S1a). Then the all-PDMS channel was cut along the channel and put on its side (Fig. S1b). At this point, uncured PDMS was applied and cured on the cut side to remove scratches from cutting. The extra PDMS smoothens the rough cut surfaces and improves the optical imaging quality. We used optical microscopy setup with extra-long working distance objective lenses (Nikon CFI Supper Plan Fluor ELWD 20×C, Nikon CFI Super Plan Fluor ELWD 40×C), which have working distance 8.2-6.9 and 3.6-2.8 mm. The channel distance from the glass slide surface could be made less than ~2 mm easily and the side-view channel and particles could be within focal length.

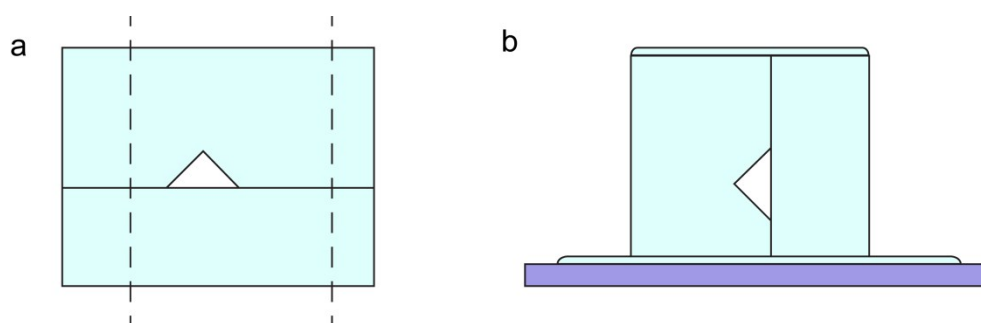
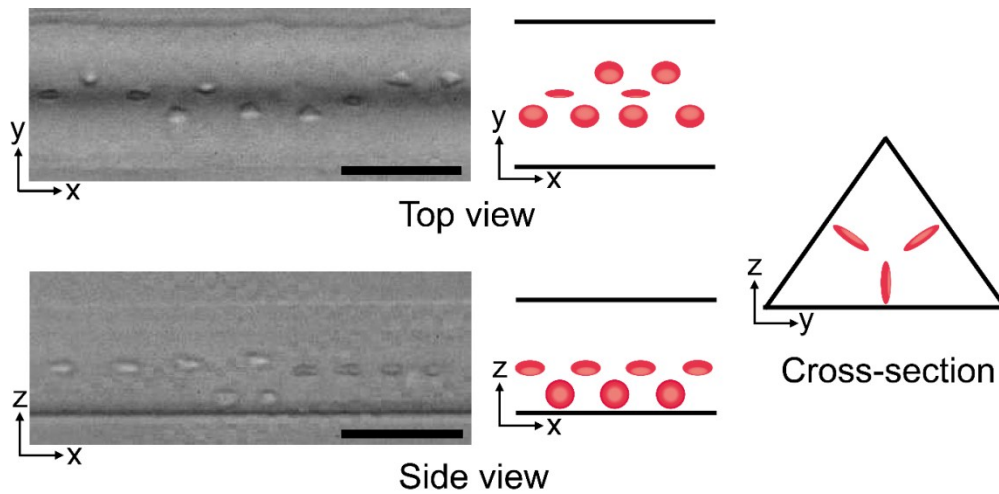


Fig. S1 Side view channel fabrication. (a) All-PDMS channel is made and cut alongside the channel. (b) The cut channel was laid on side and attached on a glass slide with extra PDMS

Inertial ordering of red blood cells in triangular channels

Disk-shaped particles in a shear flow have an easy rotation axis, which leads to alignment of the particle in specific direction. Inertially focused red blood cells show rotational ordering with four-fold symmetry in rectangular channels.¹ Similar ordering behavior is observed in triangular channels (Fig. S2). The red blood cells are focused near the center of the channel faces and the easy rotation angle align with the channel faces in the cross-sectional view.

Fig. S2 Ordering of red blood cells in a triangular channel



Inertial focusing in non-rectangular channel with various particle size

We compared inertial focusing of 7 μm and 9.9 μm diameter particles with varying R_p (Fig. S3) and found the focusing behavior is very similar. Smaller particles also have two focusing positions in half-circular channels and three shifting focusing positions in triangular channels. Exact focusing positions are somewhat different in triangular channels at the same R_p . The bottom focusing position for 7 μm particle is closer to the bottom wall, which is expected from the same size dependence of focusing position in rectangular channels. The top focusing positions of 7 μm particles are shifted more towards the lower vertices at the same R_p . As we discussed in the main text, it is necessary to achieve higher R_p to confirm when the shifting saturates, where we can exactly compare the focusing positions of different size particles.

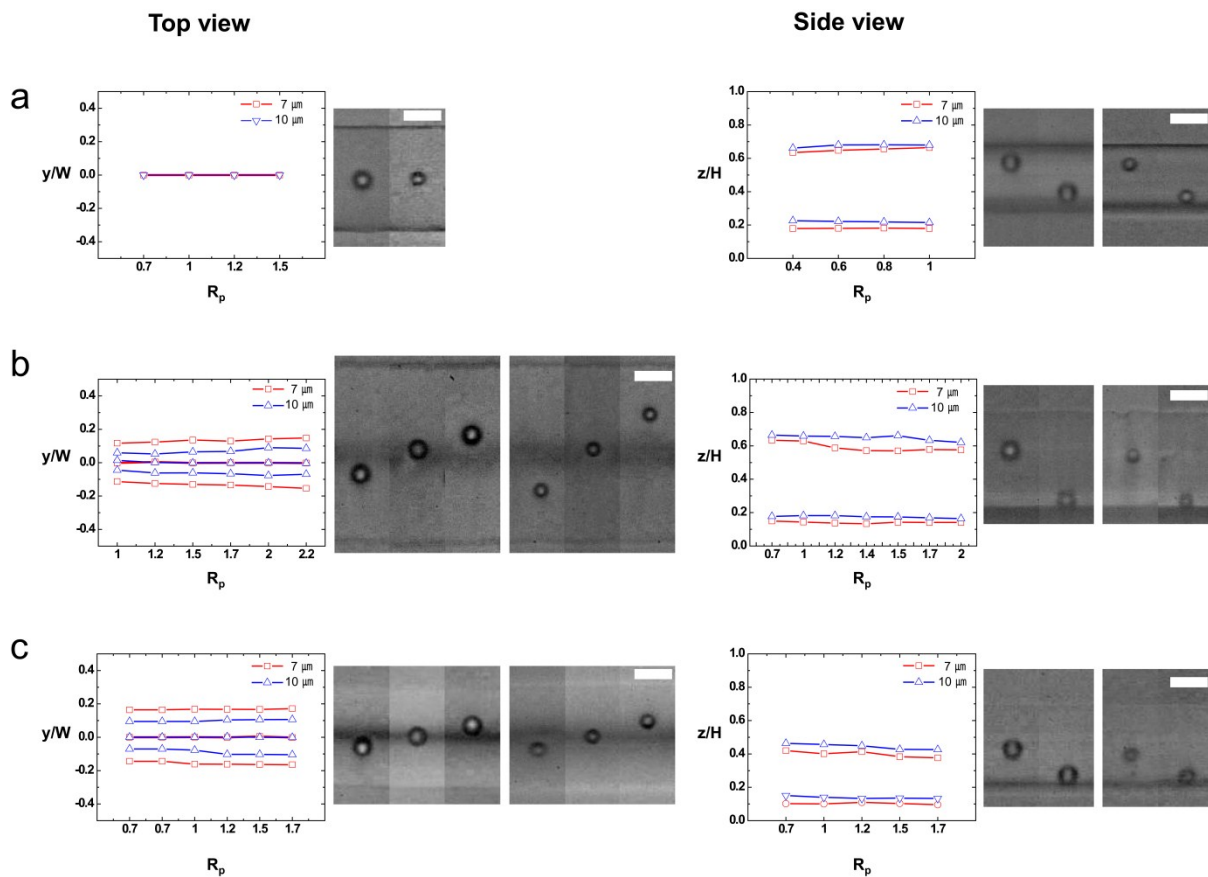


Fig. S3 Focusing positions of 7 μm and 9.9 μm diameter particles with varying R_p . (a) Half-circular (b) wide triangular (c) narrow triangular channel. (Scale bar: 20 μm)

Connection of the basins of attraction of the focusing positions in channels with varying channel cross-section

As shown in Fig. 1 and 4, microchannels have basins of attraction that lead to particle migration to each focusing position. Connection of microchannels with different cross-section leads to mismatches in focusing positions and the basins of attraction therefore the exclusion of particles in certain basins of attraction. The manipulation of particle positions using inertial focusing utilizes these mismatches. We examined the connection of stream lines within the sub-sections when the channel cross-section shape is changed.

When a rectangular channel is connected to a triangular channel, the left and right basins of attraction will be linked to the left and right side of the triangle. Fig. S4a shows stream lines that end at the basins of attraction of the top two focusing positions in the triangular channel. These stream lines cover large portion of the area near the side wall of the rectangular channel. Not only the particles focused at the two focusing positions but also particles that are not completely focused in the rectangular channel will be transported to the top basins of attraction in the triangular channel.

Fig. S4b shows the stream lines started in the top two basins of attraction of the triangular channel. The stream lines end in the upper side of the half circular channel and the focused particles in the triangular channel will eventually focus only to the top focusing position of the half circular channel.

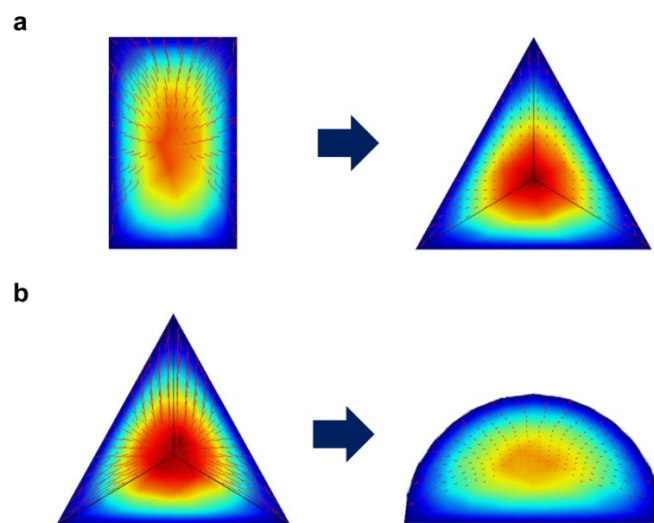


Fig. S4 Connection of basins of attraction by streamlines.

Connecting section of the single stream particle focusing device.

We observed the detailed channel geometry of the connection section for the single stream focusing device by SEM imaging (Fig. S5). The connecting section between the rectangular channel and the triangular channel has small sharp corners, where vortices can be formed. Nevertheless, the size of the dead volume is small ($< 10 \mu\text{m}$) and we don't find significant disturbance to main streamline or particle trapping to the vortices, which can be seen from the fluorescent particle streak in Fig 5. The connecting section between triangular channel and half-circular channel is relatively smooth because of the reflow process to form curved surface.

The expression for the entrance length (L_e) can be given by following equations.

For high Reynolds number²,
$$\frac{L_e}{H} \approx 0.06 \cdot Re$$

For low Reynolds number.³
$$\frac{L_e}{H} \approx \frac{0.6}{1 + 0.035Re} + 0.056 \cdot Re$$

We have $Re < 100$ and entrance length is smaller than $\sim 200 \mu\text{m}$

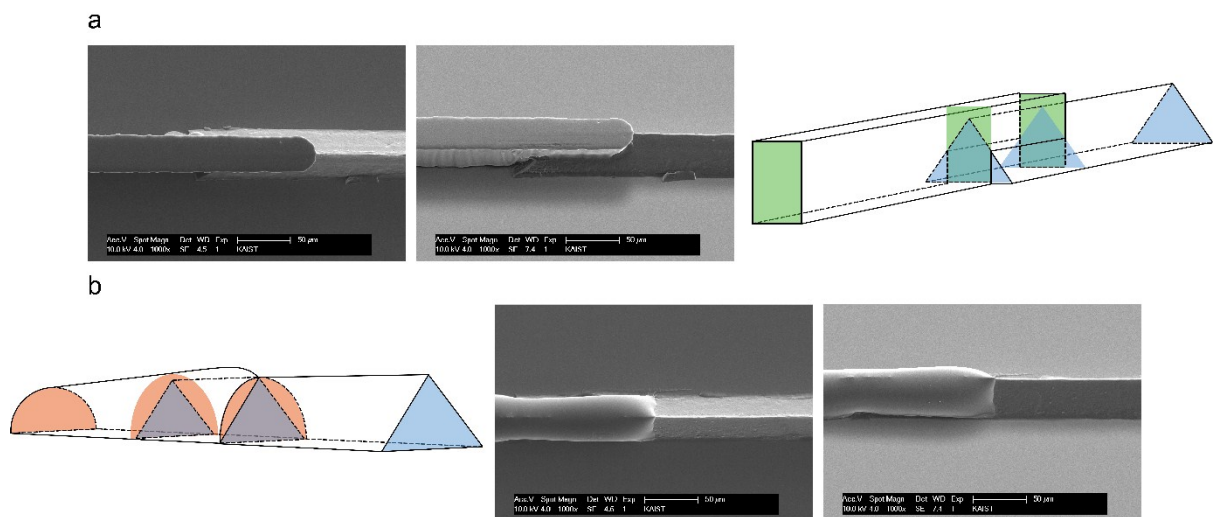


Fig. S5 SEM images and schematics of the connecting sections of a single stream focusing device. (a) Rectangular channel to triangular channel (b) Triangular channel to half-circular channel.

Computational method for force field map

We utilized a finite element method model solving the full 3D incompressible Navier-Stokes equations in COMSOL Multiphysics to simulate a spherical particle moving with the underlying fluid flow in a non-rectangular cross-section microchannel, an approach previously validated with rectangular cross-section channels.⁴ The schematics of the model geometry for triangular and half-circular channels are shown in Fig. S6. We modeled the flows in the reference frame where the particle was stationary to reduce the computational complexity. The boundary conditions (BCs) of the sidewalls were set to be a sliding velocity, $-U$, which is the velocity of the particle in the opposite direction. Inlet and outlet BCs were assigned to be the fully-developed laminar channel flows at a specified volume flow rate, Q_{ref} , which consisted of subtracting the flow from the frame of reference shift (e.g. the multiplication of the particle velocity, U , and the channel cross-section area, A) from the flow rate in the channel frame, Q , which corresponds to the experimental flow rate introduced by syringe pump. To model the rigid rotation of the particle, the particle surface was set to move tangentially (e.g. slip) at a velocity corresponding to the product of the angular velocity and radius of the particle. For each position of the particle, the slip velocities of the sidewalls and particle surface were iterated using a script until the drag force and the torque in all directions approached 0, e.g. a steady state condition for the particle moving in the flow. At this steady-state, the lateral forces induced by fluid inertia was calculated by integrating the force per area across the particle surface directed orthogonal to the flow direction.

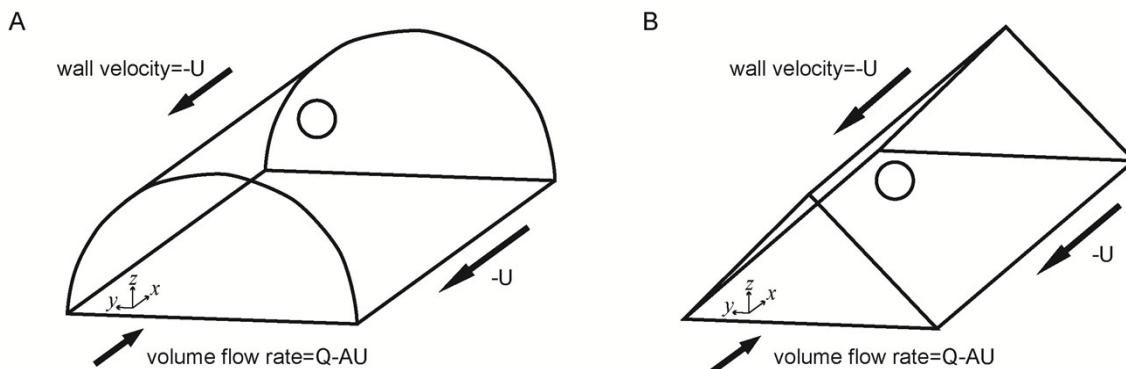


Fig. S6 Model geometry of (a) half-circular and (b) triangular channels.

References

1. D. Di Carlo, D. Irimia, R. G. Tompkins and M. Toner, *Proc. Natl. Acad. Sci. U. S. A.*, 2007, **104**, 18892-18897.
2. R. W. Fox and A. T. MacDonald, in *Introduction to Fluid Mechanics*, Wiley, 1999.
3. R. K. Shah and A. L. London, in *Laminar Flow Forced Convection in Ducts*, ed. R. K. S. L. London, Academic Press, 1978.
4. D. Di Carlo, J. F. Edd, K. J. Humphry, H. A. Stone and M. Toner, *Physical review letters*, 2009, **102**, 094503-094503.